

Preliminary Draft Report for NTSB Investigation, 4 October, 1999

**INVESTIGATION OF THE STORM ASSOCIATED WITH
THE 1 JUNE 1999 AIRCRAFT ACCIDENT AT
LITTLE ROCK ARKANSAS**

Fred H. Proctor
NASA Langley Research Center
Hampton VA

1. INTRODUCTION

American Airlines Flight 1420 crashed while landing at Little Rock National Airport at 11:51 PM CDT, 01 June 1999 (4:51 UTC 02 June). The aircraft approached the runway from the southwest, as a "bow-echo" squall line system advanced toward the airport from the west-northwest. The pilot was unable to maintain control of the aircraft following touchdown on runway 04R. Heavy rain, hail, frequent lightning, and gusty winds were observed over the airport following the time of the accident. The Low-Level Windshear Alert System (LLWAS) detected strong crosswinds prior and following the accident, and generated windshear advisories at times before and after the accident. Near the time of touchdown, the airplane may have been exposed to strong crosswinds. The center field LLWAS (located between runways 04L and 04R) reported a 10 s average wind of 41 knots (21 m/s) from 300 degrees at the time of the accident. The strongest gust was reported by the Automated Surface Observation System (ASOS), located near mid-field, with a peak wind from 320 degrees at 76 knots (39 m/s) at 4:56 UTC.

Convective weather can generate wind hazards to aviation in the form of turbulence, windshear, and strong crosswind (see Table 1). The primary focus of this analysis is to examine the available observational weather data in order to ascertain potential weather factors that may have contributed to this accident. This analysis is supplemented with numerical cloud model simulations from the Terminal Area Simulation System (TASS). A definition of windshear and its hazard characterization is given in the Appendix for reference.

2. OBSERVATIONS

A valuable source of data for analyzing this case is from the Little Rock WSR-88D weather radar, which is located approximately *14-km* north-northwest of the Little Rock Airport. The radar was able to provide Doppler velocity along the radar-beam as well as radar reflectivity fields, as the storm progressed across central Arkansas. The position of the radar relative to the airport was ideally suited for detection of the crosswind component above runway *04R*. The horizontal windshear along runway *04R*, however, could not be measured due to the beam being nearly orthogonal to the runway.

Low-level wind velocities within the terminal area were available from a six-sensor Phase-1 LLWAS. This system is capable of generating windshear advisories, although the crude spacing between sensors makes microburst windshear detection difficult (e.g., Wilson and Gramzow 1991). In addition to these sensor, an ASOS provided continuous automatic surface weather measurements at mid-field.

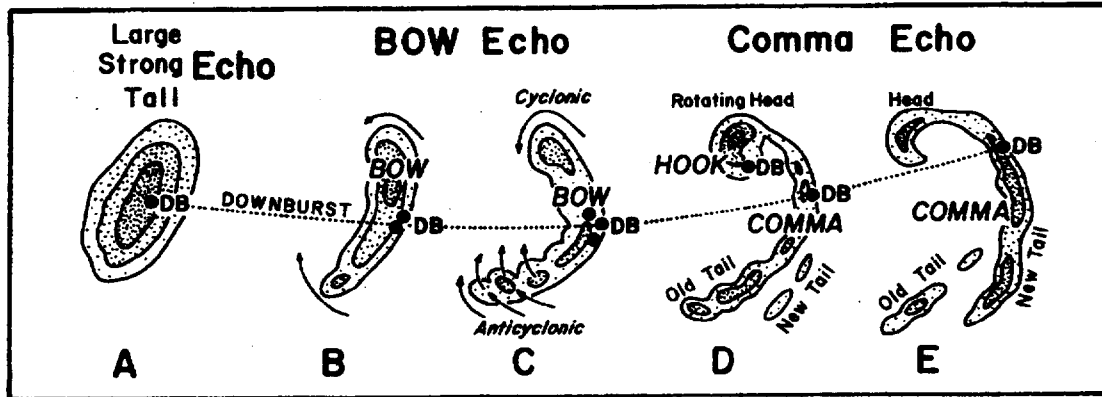


Figure 1. Evolution of radar echoes associated with a bow echo that produces a strong persistent downburst (labeled DB). The horizontal scale may range from about 10 to a few 100 km (from Fujita 1978).

The radar data showed that the severe weather near the time of the accident was associated with a “bow echo” radar signature. Bow echo signatures are known harbors of severe weather. “Bow echo” was first termed by Fujita (1978) in reference to radar echoes that appeared to undergo a forward acceleration at its midpoint, thus forming a bulge in the radar signature (see Fig. 1). This signature is similar if not identical to the Line Echo Wave Pattern (LEWP) described by Nolen (1959). Strong “straight line” winds have been known to occur near the apex of the bulge in a bow echo (Fujita 1978, Lee *et al.* 1992). In addition, other severe weather, such as downbursts and tornadoes, may accompany bow echoes (e.g., Fujita 1978, Weisman 1993).

The Little Rock radar data showed a bow echo developing west-northwest of Little Rock at 4:10 UTC. This feature was located at the northeast end of a squall line that stretched toward the southwest. The bow echo moved toward the east-southeast at about 32 knots (16 m/s), initially reaching the Little Rock airport at about 4:30 UTC. The bow echo developed a deep bulge toward the southeast as the apex of the system moved

just to the north and east of the airport. A large area of strong wind speeds in excess of 36 knots (18 m/s) was associated with low-level outflow from the bow-echo feature. Radar reflectivity exceeded 45 dBZ over a broad area, with embedded cells exceeding 60 dBZ. By 5:30 UTC, the squall line and bow-echo system had moved well east of Little Rock. A depiction of the bow echo is shown in Fig. 2.

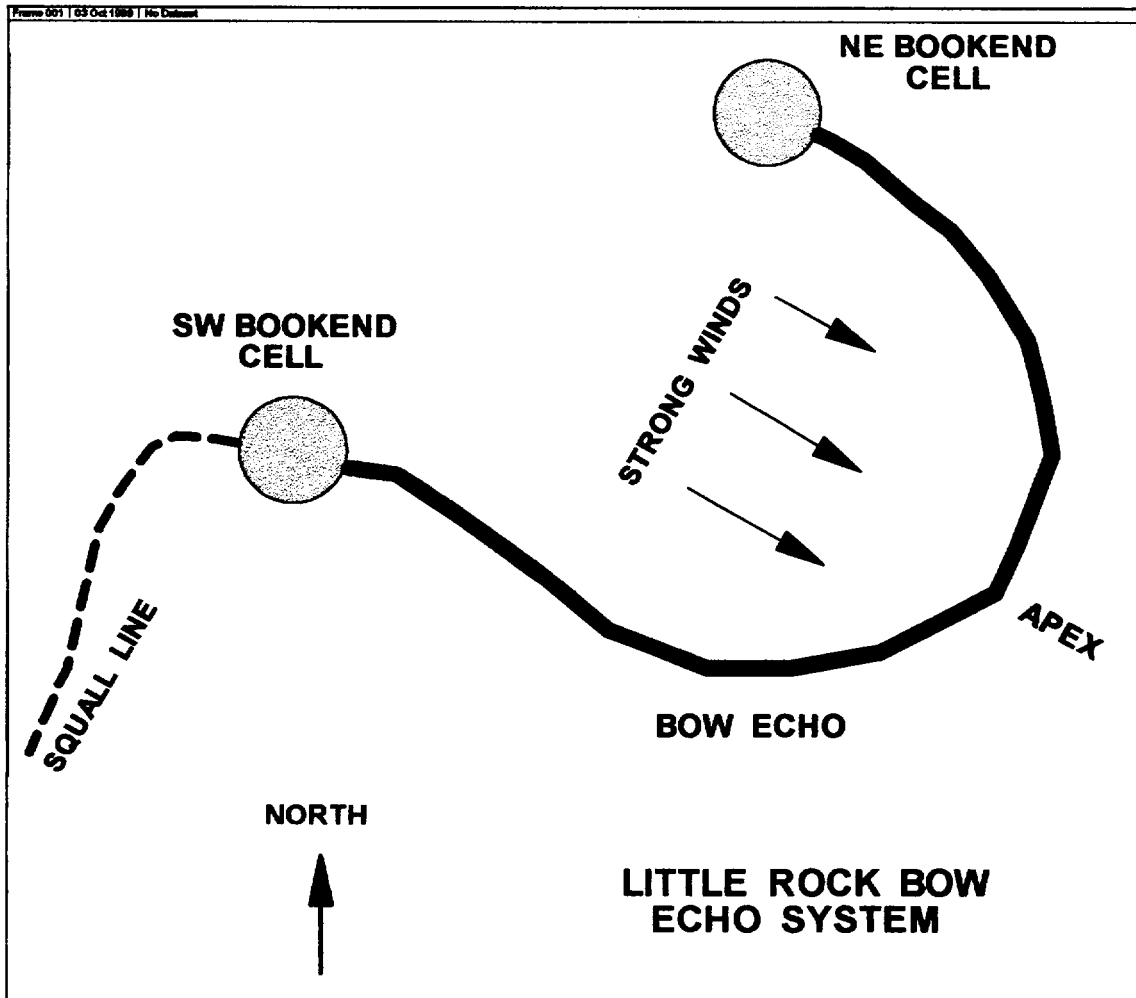


Figure 2. Depiction of bow echo system that moved across Little Rock on June 1, 1999.

Precipitation and strong wind gusts, associated with the southwestern edge of the bow echo, first reached the airport some 20 minutes prior to the time of the accident. The

southwestern edge remained near the airport as the system moved toward the east-southeast. An intense cell located at the southwestern end of the bow echo (depicted as the “SW bookend cell” in Fig. 2) moved over the airport just following the time of the accident. This cell contained radar reflectivity factor greater than 65 dBZ, and was associated with strong winds, hail, frequent lightning, and high rainfall rates as it passed over the airport. A peak rainfall rate of 9 inches/hr (0.15 in/min) was recorded by ASOS at 4:56 UTC with the passage of this cell. During this time, the strongest measured gust of 76 knots was reported by the ASOS anemometer. The Doppler radar also showed strong winds from this cell. It measured winds over the airport in excess of 47 knots (24 m/s).

3. NUMERICAL MODEL SIMULATION

Numerical simulation of this event using a numerical cloud model may be useful for providing additional insight into the role weather might have played. The model that is used is called the Terminal Area Simulation System (TASS) (e.g., Proctor 1987a, 1996). TASS is a three-dimensional, Large-Eddy Simulation model and includes parameterizations for both liquid- and ice-phase microphysics. The model played an important role in NASA's recent windshear program (Arbuckle *et al.* 1996; Airborne Windshear Detection and Warning Systems, 1988, 1990, 1991, 1992, 1994), and has been applied to a diversity of microburst windshear cases (Proctor 1987b, 1988a,b, 1989, 1992, 1993; Proctor and Bowles 1992). The model also was applied in a previous NTSB investigation (Proctor 1994, Proctor *et al.* 1995) and has supplied the FAA with a variety of model-generated data sets for use in industry certification of look-ahead windshear systems (Switzer *et al.* 1993).

3.1 INITIAL CONDITIONS

The time-dependent simulation is performed in three-dimensions assuming 55 vertical levels with each level resolved by a 175×175 point grid mesh. The assumed grid size was 333.33 m in the horizontal and a stretched grid size in the vertical extending from the ground to an altitude of 18 km . This grid size allows resolution of eddies and scales of motion that are larger than 333.33 m .

Successful simulation of an observed event with the TASS model requires an input sounding representative of the local storm environment. The vertical profiles of ambient wind, humidity and temperature are quite crucial in determining both storm structure and storm intensity. The rawinsonde sounding launched at Little Rock at 0000 UTC was first examined as input for the simulation. However, it was believed unrepresentative due to the capping inversion and shallow depth of the moist layer. Since rawinsonde soundings are launched only every 12 hours, a forecast sounding was requested from the NOAA Forecast Systems Laboratory. This sounding (Fig. 3 and Table 2) was generated from the operational Mesoscale Analysis and Prediction System (MAPS) model (Benjamin *et al.* 1996) for 4:00 UTC at Little Rock. However, sustained convection could not be generated with this sounding. A subsequent sounding (Fig. 4) was produced by matching the MAPS sounding with observed surface conditions at Little Rock, and simulating the effect of evaporating snow and ice crystals as might be expected due to the over-running of clouds from mid- and upper-level storm blow-off (e.g. see, <http://cimss.ssec.wisc.edu/goes/misc/990602.html>). All simulation results described below are from the TASS simulation with ambient conditions represented by Fig. 4.

Convection, which evolved into the simulated bow-echo system, was initiated by a thermal ellipsoid. No attempt, otherwise, was made to include horizontal variations of the ambient flow field and to simulate the squall-line cells adjacent to the southwestern end of bow echo (see Fig. 2).

3.2 RESULTS

Results from TASS with the initial conditions shown in Fig. 4 contain similarities to the observed case (Table 3), but also, important discrepancies (Table 4). The results do allow us to infer the potential for strong winds, windshear, and heavy precipitation within the Little Rock environment. However, a detailed and accurate reconstruction of the accident from the simulation was not possible.

Plots of radar reflectivity and horizontal wind vector from the simulation are shown at three different simulation times in Figs. 5-10. [The simulation time is in reference to the start of the simulation.] In these plots, north is in the direction of the y-coordinate and east is in the direction of the x-coordinate.

Figures 5, 7, and 9 show a horizontal cross section of the simulated low-level radar reflectivity field at 85, 95, and 110 min. A bow shaped echo is produced with a pair of strong "bookend cells" (e.g., Weisman 1993) on the *NE* and *SW* sides. These cells are apparent by their local values of high radar reflectivity. The precipitation cores within these cells are greater than 60 *dBZ*. The *SW* bookend cell was the most intense, and was accompanied by simulated rainfall rates of 8 inches per hour. The apex of the simulated bow echo is directed toward the southeast; but unlike the radar observations, a continuous band of strong reflectivity did not outline the southeastward bulge of the radar signature.

In addition, the observation showed one or more intense cells near the apex, and a broad region of radar reflectivity greater than 45 dBZ . Because of the inability of this simulation to capture these features, the strong northwesterly surface outflow was not simulated under the bowing region of the radar signature (cf. Figs. 6, 8, and 10.). Large-scale downbursts or macroburst, were associated with the simulated bookend cells. The simulated downbursts had horizontal scales of $\sim 10\text{-}20 \text{ km}$. Peak low-level winds exceeded 30 m/s with the downbursts, but hazardous levels of windshear were confined to very small areas within the high precipitation cores of the bookend cells. Peak horizontal wind changes over any 4-km segment exceeded 32 m/s , but the maximum 1-km averaged F-factor rarely exceeded 0.15 (as based on level flight paths with an air speed of 70 m/s , see appendix). The size, speed and direction of the bow-echo system were similar between simulation and observation (Table 3). Both observation and simulation indicated a significant temperature drop under the intense cells, even though a cool nocturnal stable layer was present. The simulation also revealed a strong mesocyclonic circulation (sometimes a predecessor for tornadoes) within the *SW* bookend cell, but this has not been verified from the observations. Little Rock and the surrounding area were under a tornado watch when the storm moved through.

The simulation revealed that the environment had a propensity to produce a severe bow-echo system, with large-scale downbursts, strong outflow winds, heavy rainfall and hail. But due to the large scale of the downburst, the windshear was only marginally hazardous, and confined to the precipitation cores; i.e., regions of high reflectivity where aircraft usually avoid anyway, due to poor visibility and the threat of hail. The horizontal scale of the downbursts associated with this environment were generally much larger than

those in windshear cases we had previously examined (e.g., Proctor 1988, 1988b, Proctor and Bowles 1992, Proctor *et al.* 1995).

4. SUMMARY AND CONCLUSIONS

A strong bow-echo event approached the airport during the time of the accident. This feature is a known harbinger of severe weather and can be detected with conventional and Doppler radar. The bow-echo system produced strong crosswinds, which could hamper the safe landing and departing of aircraft.

Although the system produced strong downburst with damaging winds, hazardous levels of windshear were probably confined to near the center of the precipitating cores. These areas would not be normally encountered by aircraft due to their high reflectivity level and potential for hail. Since the accident aircraft approached from the southwest, it may not have encountered the intense precipitation cores with their potential for hazardous windshear.

5. SUGGESTIONS/OPINIONS

Based on the analysis of this case and my knowledge in this area:

- i.) *The hazard from crosswind and windshear should not be treated as synonymous. The affect of crosswind on aircraft control is different than from windshear (see Table 1). Also, regions of hazardous crosswinds do not overlay regions of hazardous windshear. Some meteorological conditions may produce either but not both.*

- ii.) *On board, look-ahead windshear sensors do not detect hazardous crosswind on approach since these systems primarily detect the component of wind along the direction of the flight path.*
- iii.) *Terminal Doppler Radar Weather Radar (TDWR) and LLWAS may issue gust front advisories, but I am not aware of the dissemination of products for hazardous crosswind. However, such products could be developed.*
- iv.) *Advisories and alerts for hazardous crosswind could be easily developed and implemented into existing LLWAS systems.*

Acknowledgments

The atmospheric sounding from the Mesoscale Analysis and Prediction System (MAPS) forecast model was provided by Stan Benjamin of NOAA Forecast Systems Labs. All other weather and accident data was provided by NTSB.

Table 1. Comparison between turbulence, windshear, and crosswind threats to aircraft.

Hazar

Turbulence Threat

Definition: *encounter with man-made or atmospheric scales of motion that cause intense, short-lived, random accelerations on the aircraft.*

Hazard: 1) *passengers and crew subject to unexpected and violent aircraft accelerations that cause injury or death;*
2) *loss of control and possible aircraft upset, resulting in uncontrolled flight into terrain;*
3) *lack of control authority on touchdown resulting in damage to aircraft;*
4) *airborne damage to aircraft.*

Phase of flight: *can occur at any altitude, and during all phases of flight.*

Windshear Threat

Definition: *encounter with atmospheric events that cause critical reduction in airspeed or altitude, such as to threaten the ability of an aircraft to remain airborne.*

Hazard: *flight into terrain.*

Phase of flight: *low altitude, during approaches and departures.*

Crosswind Threat

Definition: *strong crosswinds that may endanger the control and course of the aircraft during takeoff and landings.*

Hazard: *collision with obstacles, lack of control authority on touchdown resulting in damage to aircraft and injury to passengers, impaired directional control on the runway.*

Phase of flight: *on runway and at low altitude during approaches and departures.*

Table 2. Tabulated data from MAPS forecast sounding shown in Fig. 3.

Pressure (ft)	Alt (mb)	DD	Dir	Spd (kts)	---Temp---		DewPt (C)
					(F)	(C)	
354	999.0	A	159	7	77.5	25.3	22.3
426	996.0	A	171	10	77.5	25.3	22.1
570	991.0	A	178	13	77.0	25.0	21.6
790	984.0	A	184	18	76.6	24.8	21.0
1085	974.0	A	192	23	76.6	24.8	20.2
1532	959.0	A	201	29	77.4	25.2	20.7
1984	944.0	A	207	32	75.7	24.3	20.2
2444	929.0	A	214	32	73.8	23.2	19.4
2585	925.0	A	216	32	73.0	22.8	19.1
2910	914.0	A	219	31	71.2	21.8	18.4
3382	899.0	A	223	31	69.6	20.9	18.0
3858	884.0	A	228	32	67.6	19.8	17.4
4340	869.0	A	234	32	65.5	18.6	16.7
4829	854.0	A	235	31	63.5	17.5	16.0
4986	850.0	A	237	30	63.1	17.3	15.8
5328	839.0	A	242	29	62.4	16.9	15.5
5830	824.0	A	248	27	61.3	16.3	14.3
6345	809.0	A	252	27	60.4	15.8	12.9
6863	794.0	A	249	26	59.0	15.0	11.1
7391	779.0	A	247	25	57.4	14.1	9.2
7929	764.0	A	248	24	55.4	13.0	7.4
8474	750.0	A	253	24	53.4	11.9	5.5
9025	735.0	A	255	28	52.3	11.3	3.5
9589	720.0	A	254	34	50.4	10.2	0.8
10160	705.0	A	250	34	48.2	9.0	-2.6
10357	700.0	A	252	34	47.5	8.6	-3.6
11555	669.0	A	264	33	43.5	6.4	-10.5
14580	597.0	A	276	34	31.1	-0.5	-19.3
16797	548.0	A	277	35	22.5	-5.3	-29.0
18369	515.0	A	279	32	17.2	-8.2	-34.9
19163	500.0	A	282	34	14.9	-9.5	-36.8
19862	486.0	A	284	36	12.4	-10.9	-38.7
22703	433.0	A	274	38	1.2	-17.1	-42.9
24671	400.0	A	273	34	-6.7	-21.5	-45.2
26043	378.0	A	272	32	-12.5	-24.7	-47.0
28854	335.0	A	272	28	-23.4	-30.8	-49.1
31407	300.0	A	277	21	-34.1	-36.7	-50.4
32191	289.0	A	278	19	-37.5	-38.6	-50.9
34780	258.0	A	259	10	-47.6	-44.2	-54.4
35475	250.0	A	267	13	-49.5	-45.3	-55.9
36955	233.0	A	283	18	-54.4	-48.0	-59.3
39445	208.0	A	283	30	-60.7	-51.5	-66.5
42450	180.0	A	287	32	-67.7	-55.4	-71.0
44468	163.0	A	274	23	-68.8	-56.0	-78.6
46279	150.0	A	270	30	-72.6	-58.1	-81.4
48116	137.0	A	266	37	-76.9	-60.5	-84.5
54442	100.0	A	284	19	-90.4	-68.0	-81.9
55764	93.0	A	288	15	-93.5	-69.7	-81.5

66000 55.0 A 20 10 ***** -76.6 -80.1

Table 3. Similarities between simulated and observed features of the bow-echo system.

Similarities of Bow-Echo System		
<i>Parameter</i>	<i>Observed</i>	<i>Modeled</i>
Movement	16 m/s at 300°	18 m/s at 282°
Width	~40 km	~50 km
Orientation of Apex or Bulge	NW to SE	NW to SE
Horizontal Depth Along Apex	~40 km	~40 km
Peak Radar Reflectivity	>65 dBZ	73 dBZ
Peak Rainfall Rate	9 inches/hr	8 inches/hr
Hail	yes	yes
Peak Outflow Wind	ASOS: 39 m/s, RADAR: greater than 35 m/s	30 m/s (mean wind over 333.3 m grid)
Minimum Surface Temp	19° C	17° C
Duration	Persistent, multi-cellular	Persistent, multi-cellular

Table 4. Major differences between simulation and observed event.

Major Shortcomings of Numerical Simulation
<i>Bow-echo comprised of a few broken cells rather than solid line of cells.</i>
<i>Bow-echo is not sharply defined as in observations. Missing strong band of reflectivity along the edge of the bulge.</i>
<i>Area covered by 45 dBZ reflectivity underestimated.</i>
<i>Did not capture the broad area of strong surface outflow near apex of the bow echo.</i>

References

Airborne Windshear Detection and Warning Systems. 1988. First Combined Manufacturers' and Technologists' Conference, NASA CP-10006, DOT/FAA/PS-88/7.

Airborne Windshear Detection and Warning Systems. 1990. Second Combined Manufacturers' and Technologists' Conference, NASA CP-10050.

Airborne Windshear Detection and Warning Systems. 1991. Third Combined Manufacturers' and Technologists' Conference, NASA CP-10060, DOT/FAA/RD-91/2-1.

Airborne Windshear Detection and Warning Systems. 1992. Fourth Combined Manufacturers' and Technologists' Conference, NASA CP-10105, DOT/FAA/RD-92/19-1.

Airborne Windshear Detection and Warning Systems. 1994. Fifth and Final Combined Manufacturers' and Technologists' Conference, NASA CP-10139, DOT/FAA/RD-94/14-1.

Arbuckle PD, Lewis MS, Hinton DA. 1996. Airborne systems technology application to the windshear threat, 20th Congress of the International Council of the Aeronautical Sciences, ICAS Paper No. 96-5.7.1, pp. 1640-1650.

Benjamin SG, Brown JM, Brundage KJ, Devenyi D, Schwartz B, Smirnova TG, Smith TL, Wang F-J. 1996. The 40-km 40-level version of MAPS/RUC. Preprints, 11th Conference on Numerical Weather Prediction, Norfolk, August, 161-163.

Bowles RL. 1990a. Reducing windshear risk through airborne systems technology. The 17th Congress of the ICAS, Stockholm, Sweden, 27 pp.

Bowles RL. 1990b. Windshear detection and avoidance – airborne systems survey. 29th IEEE Conf. on Decision and Control, 2:708-736.

Federal Aviation Administration. 1987. *Wind Shear Training Aid*. (Available from NTIS as PB88-127196).

Frost W, Bowles RL. 1984. Wind shear terms in the equations of aircraft motion. *J. Aircraft* 21:866-872.

Fujita TT, Byers HR, 1977. Spearhead echo and downburst in the crash of an airliner. *Mon. Wea. Rev.* 105: 129-146.

Fujita TT. 1978. Manual on downburst identification for project NIMROD. Satellite and Mesometeorology Research Paper No. 156, Dept. of Geophysical Sciences, Univ. Chicago, 104 pp. [NTIS PB-286048]

Fujita TT. 1985. *The Downburst, Microburst and Macroburst*. University of Chicago Press, 154 pp.

Hinton DA. 1990. Relative merits of reactive and forward-look detection for wind shear encounters during landing approach for various microburst escape strategies. NASA TM-4158, DOT/FAA/DS-89/35.

Hinton DA. 1992. Forward-look wind shear detection for microburst recovery. *J Aircraft* 29:63-66.

Hinton DA. 1994. Flight test evaluation of a data link and aircraft integration of TDWR wind-shear information. *Airborne Windshear Detection and Warning Systems. 1994. Fifth and Final Combined Manufacturers' and Technologists' Conference*, NASA CP-10139, DOT/FAA/RD-94/14-1, 23-48.

Lee W-C., Wakimoto RM, Carbone. 1992. The evolution and structure of a "bow-echo-microburst" event. part II: the bow echo. *Mon. Wea. Rev.* 120:2212-2225.

Lewis MS, Robinson PA, Hinton DA, Bowles RL. 1994. The relationship of an integral wind shear hazard to aircraft performance limitations. NASA TM-109080.

Nolen RH. 1959: A radar pattern associated with tornadoes. *Bull. Amer. Meteor. Soc.*, 40:277-279.

Proctor FH. 1987a. The Terminal Area Simulation System. Volume I: theoretical formulation. NASA Contractor Rep. 4046, NASA, Washington, DC, 176 pp.

Proctor FH. 1987b. The Terminal Area Simulation System. Volume II: verification experiments. NASA Contractor Rep. 4047, NASA, Washington, DC, 112 pp.

Proctor FH. 1988a. Numerical simulations of an isolated microburst. Part I: dynamics and structure. *J. Atmos. Sci.*, 45:3137-3160.

Proctor FH. 1988b. Numerical simulation of the 2 August 1985 DFW microburst with the three-dimensional Terminal Area Simulation System. Preprints Joint Session of 15th Conf. on Severe Local Storms and Eighth Conf. on Numerical Weather Prediction, Baltimore, Amer. Meteor. Soc., J99-J102.

Proctor FH. 1989. Numerical simulations of an isolated microburst. Part II: sensitivity experiments. *J. Atmos. Sci.*, 46:2143-2165.

Proctor FH. 1992. Three-dimensional numerical simulation of the 20 June 1991, Orlando Microburst. Airborne Wind Shear Detection and Warning Systems, Fourth Combined Manufacturers' and Technologists' Conference, Williamsburg, VA., NASA CP-10105, Part 1, 213-242.

Proctor FH. 1993. Case study of a low-reflectivity pulsating microburst: numerical simulation of the Denver, 8 July 1989, storm. Preprints, 17th Conf. on Severe Local Storms, St. Louis, Missouri, Amer. Meteor. Soc., 677-680.

Proctor FH. 1994. Investigation of microburst windshear associated with the Charlotte 1994 accident using a meteorological numerical model. National Transportation Safety Board, Docket No. SA-509, Exhibit No. 5-I, 31 pp.

Proctor, FH. 1996. Numerical simulation of wake vortices measured during the Idaho Falls and Memphis field programs. 14th AIAA Applied Aerodynamics Conference, Proceedings, Part-II, 17-20 June, New Orleans, LA, AIAA Paper No. 96-2496, 943-960.

Proctor FH, Bowles RL. 1992. Three-dimensional simulation of the Denver 11 July 1988 microburst-producing storm. *Meteorol. and Atmos. Phys.*, 49:107-124.

Proctor FH, Bracalente EM, Harrah SD, Switzer GF, Britt CL. 1995. Simulation of the 1994 Charlotte microburst with look-ahead windshear radar. Preprints, 27th Conference on Radar Meteorology, Amer. Meteor. Soc., 530-532.

Switzer GF, Proctor FH, Hinton DA, Aanstoos JV. 1993. Windshear database for forward-looking systems certification. NASA TM -109012, 133 pp.

Targ R, Bowles RL. 1988. Investigation of airborne lidar for avoidance of windshear hazards. AIAA-88-4658, 9 pp.

Weisman ML. 1993. The genesis of severe, long-lived bow-echoes. *J. Atmos. Sci.*, 50:645-670.

Wilson FW Jr, Gramzow RH. 1991. The redesigned Low Level Wind shear Alert System. Preprints, Fourth Intl. Conf. on the Aviation Weather System, Paris, Amer. Meteor. Soc.

Wilson JW, Roberts RD, Kessinger C, McCarthy J. 1984. Microburst wind structure and evaluation of Doppler radar for airport wind shear detection. *J. Climate Appl. Meteor.*, 23: 898-915.

Appendix: WINDSHEAR
(Fred H. Proctor and David A. Hinton)

A.1. DEFINITION OF WINDSHEAR

In the context of aviation science, windshear refers to a wind speed or direction change experienced by an airplane over a particular distance or length of time. This definition covers an extremely wide range of meteorological phenomena, including convective turbulence, gust fronts, microburst, internal gravity waves, vertical shear (such as due to low-level atmospheric jetstreams), and terrain-influenced flow. Some of these events are merely nuisances, leading to poor ride quality, increased pilot-workload, or rough landings. However, an aircraft exposed to windshear of sufficient intensity and duration, may lose flight performance with a reduction of airspeed or flight altitude. Windshear is deemed hazardous when it has the potential to reduce an aircraft's energy state at a rate faster than can be added back by engine thrust, and thus endangering the aircraft by either reducing its airspeed below stall speed or by diminishing its elevation above the ground. This danger is limited to departing and arriving aircraft, since at this phase of flight, aircraft carry minimal excess energy and are at low altitude and airspeed. Moreover, the potential hazard to departing and arriving aircraft is made more critical by the aircraft's flight configuration of landing gear and flap settings, which require time to reconfigure in order to gain maximum thrust.

A.2 WINDSHEAR HAZARD INDEX

Before discussing the phenomenology that is associated with hazardous windshear, it is first instructive to define a general metric that quantifies the windshear threat. Such an index was developed by Bowles (1990a, 1990b), based on the fundamentals of flight

mechanics and the current understanding of windshear phenomena. This index, known as the F-factor, incorporates observable atmospheric parameters, and scales with aircraft flight performance in such a way as to predict impending flight path deterioration.

The concept employed in the derivation of the F-factor is the total aircraft energy and its rate of change. The total aircraft energy is simply the sum of the air-mass relative kinetic energy (airspeed) and the internal potential energy (altitude above the ground).

The aircraft total specific energy (energy per unit mass) is defined as $E_T = h + \frac{1}{2} \frac{V^2}{g}$

where V_a is airspeed, g is gravitational acceleration, and Z is altitude above ground. The above relationship uses air-mass kinetic energy, since airspeed, not ground speed, describes an airplane's ability to climb and maintain altitude. Likewise, inertial potential energy is used since altitude above the ground is most important to an airplane. The time rate of change of E_T (which is also the potential rate of climb of the aircraft), can be equated with the aircraft energy input from thrust and drag, as:

$$\frac{dE_T}{dt} = \frac{V}{g} \frac{dV}{dt} = \frac{V(T-D)}{W} \quad (1)$$

where $(T - D) / W$ is the ratio of the aircraft thrust minus drag to weight; i.e. the excess thrust to weight capability of the aircraft. Note that when thrust equals drag the aircraft will maintain a constant speed and altitude, or the pilot may maneuver to exchange aircraft potential energy for kinetic energy. The above relationship is valid for a uniform airmass only. The effect of variable atmospheric wind fields can be included by combining Equation (1) with the appropriate aircraft equations of motion (e.g., Frost & Bowles 1984). Neglecting second-order terms, the new relationship becomes:

$$\dot{E}_T = \dot{E}_+ \frac{V \dot{U}_x}{g} = \frac{V(T-D)}{W} \quad (2)$$

where U_x is the component of atmospheric wind directed horizontally along the flight path, \dot{U}_x is the time rate of change of U_x experienced by the aircraft, and w is the updraft within the airmass. In Equation (2), the wind-field terms constitute a nondimensional parameter defined by Bowles (1990a, 1990b) as the *F-factor*:

$$F \equiv \frac{\dot{U}_x}{g} - \frac{w}{V_a} \quad (3)$$

Note from Equation (2) that a positive F-factor acts to decrease the energy state of an aircraft; the F-factor is positive for a descending air mass ($w < 0$) and a wind field accelerating in the direction of the flight path ($\dot{U}_x > 0$). In the absence of airmass vertical motion, performance-decreasing shears ($\dot{U}_x > 0$) act to decrease the energy state of the aircraft, while performance-increasing shear ($\dot{U}_x < 0$) act to increase the energy state.

The shear term, \dot{U}_x , in Equations (2) and (3), is a function both of the meteorological event and the aircraft trajectory, e.g.,

$$\dot{U}_x = \frac{\partial W_x}{\partial x} \dot{x} + \frac{\partial W_x}{\partial h} \dot{h} + \frac{\partial W_x}{\partial \alpha} \quad (4)$$

Both horizontal and vertical shears contribute to the shear term. The first term in Equation (4) is the product of the horizontal shear directed along the flight path and the aircraft ground speed. This term is the primary contributor to aircraft performance loss during most accident encounters. The second term is the product of the vertical change of horizontal wind and the aircraft ascent rate. This term predominates when the aircraft climbs or descends through strong vertical shears, but has no contribution for level flight.

The final term is the local rate-of-change of horizontal wind with time, which usually has only secondary importance during typical windshear encounters. Rearranging terms in Equation (2), the change in airspeed is:

$$\dot{V} = \dot{V}_w + \frac{V \dot{W}}{g} = \frac{V(T-D)}{W} \quad (5)$$

Note that a loss of airspeed in a performance-decreasing shear (with $F > 0$), can be minimized by an increase in thrust and a reduction in altitude. For a strong shear that exceeds the thrust capability of the aircraft, i.e., $F > (T_r - D)/W$, a pilot may either manage his flight so as to maintain altitude while decelerating, maintain airspeed while descending, or some compromise of the two. At low altitude during takeoff or landing, the speed margin above aerodynamic stall speed is minimal and the height is critical. Numerous studies have been conducted (e.g., Hinton 1990, 1992) on optimal and practical techniques for escaping a windshear encounter. The recommended procedure in use today (Federal Aviation Administration 1987) results in extracting the maximum performance from the aircraft and maximizing the likelihood of exiting the windshear event prior to stalling or making ground contact.

The excess thrust-to-weight capability varies by aircraft type. For a 4-engine jet aircraft, the ratio may be about 0.10 at full thrust and maximum takeoff weight. Due to the thrust requirements for engine-out climb performance, 3- and 2-engined aircraft have higher performance than 4-engine aircraft. A typical 3-engine jet transport may have an excess thrust to weight ratio of 0.13 or more, while a twin-engine may exceed 0.17. Hence, by applying excess thrust, jet aircraft are capable of maintaining their energy state for conditions with $F < 0.10$. The situation becomes more critical for an unexpected

windshear encounter on landing approach. The excess thrust to weight ratio is about - 0.05 for a typical approach on a 3-degree glide slope (as would be the case prior to detection of the windshear event). Upon an unexpected encounter, significant total energy can be lost from the aircraft during the 5 to 10 seconds of time required to recognize the threat and reach full thrust.

Typical piston-engine general aviation aircraft have excess thrust to weight ratios of about 0.10 to 0.15 , and can reach full thrust in a shorter time than jet aircraft. As is apparent from Equations (2) - (4), the slower airspeed of piston aircraft reduces the impact from horizontal and vertical shear, but increases the significance of vertical winds. Hence, an atmospheric event considered hazardous to jet aircraft may not be so for a piston-driven aircraft, and *vice versa*.

A.3 HAZARD THRESHOLDS

Since Equations (2)-(5) only describe the instantaneous effect of shear on aircraft specific energy and airspeed, the equations must be integrated over an appropriate scale length to characterize the hazard of the event. For example, very large magnitudes of F may occur for brief moments from turbulence associated with the convective planetary boundary layer, but the positive values of F are over small length scales and are quickly followed by negative values. Such oscillations of F-factor result in perceived turbulence, with airspeed oscillations and little net trajectory change. Air motion associated with very-high frequency oscillations of F-factor may even exceed the ability of the aircraft to respond. Thus, in order for the F-factor to be useful as a hazard metric it must be averaged or computed in such a way, so as to represent a significant deterioration in flight

path. Such an effort was conducted by Lewis *et al.* (1994). They proposed that the F-factor be averaged over some given horizontal extent (L) as:

$$\bar{F}(s_0, L) = \frac{1}{L} \int_{s_0}^{s_0+L} F ds = \frac{1}{L} \int_{s_0}^{s_0+L} \left(\frac{T-D}{W} \right) ds - \frac{\Delta(V^2)}{2gL} - \frac{\Delta h}{L} \quad (7)$$

where the right side of Equation (7) relates an average F-factor to the airplane performance capability lost over the spatial extent L . From (7) it is possible to determine the magnitude and spatial extent that the aircraft can survive, given specific initial energy conditions (speed and height) and allowable energy loss. Calculations were performed by Lewis *et al.* for a range of cases in order to identify a minimum hazard threshold for \bar{F} and an appropriate minimum length scale (L) for windshear exposure. To perform this calculation, their assumptions included a profile of $(T, -D)/W$ for a specific aircraft type on approach as well as for departure. Each profile began with a value appropriate for either the take-off or landing phase of flight (maximum for the airplane for takeoff and -0.05 for landing approach), then a delay interval for pilot recognition of the shear (thrust does not change), followed by a thrust ramp up period (the excess thrust to weight ratio linearly increases to the maximum value). The pilot recognition delay period was assumed to begin at entry into the shear, and maximum $(T, -D)/W$ was reached at the time indicated by the sum of the pilot delay and the engine ramp up. This calculation was done for a number of airplane types representing a range of conventional jet transport aircraft, and was based on realistic but conservative data. The limiting case, representing a worst case low-altitude encounter, required a 1-km length scale and an average F of 0.12 or greater. The Federal Aviation Administration (FAA) has adopted the 1-km average F-factor as its hazard metric for windshear surveillance systems on jet transports, and

considers windshear hazardous for $\bar{F} \geq 0.1$, and a *must alert* threshold at 0.13 (e.g., Hinton 1994).

A.4 ATMOSPHERIC WINDSHEAR PHENOMENA

The threat from low-altitude windshear is limited to those atmospheric phenomena that maintain a significant level of shear over a particular range of scales. Phenomena with high levels of F , but over short distances (horizontal scales less than 400 m), are experienced as turbulence by jet aircraft. Phenomena with wind shear distributed over large length scales (of order 10 km and greater) are unlikely to have magnitudes of shear that would directly affect the safety of an aircraft. However, those events having a mid-range of scales, *i.e.* horizontal scales of approximately 400 to 4000 m , are most likely to impact the performance of departing and arriving aircraft. The primary atmospheric phenomenon that can produce hazardous low-altitude windshear within this range of scales are microbursts. Since the late 1970's when microburst phenomenon were first recognized as threat to aviation (e.g., Fujita and Byers 1977), the vast majority of windshear accidents and incidents involving jet transports have been attributed to microburst windshear.

A.5 MICROBURSTS AND MACROBURSTS

A microburst is loosely defined as an intense local downdraft with divergent surface outflow. Microbursts are always associated with precipitation from convective clouds, and may produce magnitudes of vertical velocity and horizontal shear that can threaten landing and departing aircraft. The winds from intense microbursts may even cause wind damage to ground structures (e.g., Fujita 1985). Radar meteorologists identify surface outflows as microburst when their peak horizontal divergence exceeds 10

m/s within a 1-4 km segment (e.g. Wilson *et al* 1984). Divergent outflows with horizontal scale greater than 4 km are termed macrobursts (Fujita 1985), although they may contain one or more embedded microbursts. A “downburst” refers to either a microburst or a macroburst.

Not all microburst may achieve intensities that are a hazard to commercial aviation. From a 251 microburst sample, Bowles (1990a) points out that approximately half would not qualify as a threat, as based on a hazard threshold for average F-factor of 0.1. Values for average F-factor from microburst accident encounters range from about 0.2 to 0.36 (Targ & Bowles 1988, Proctor *et al.* 1995). The magnitude of these values exceeds the performance capability of most aircraft, and indicates the severity of the windshear threat from *intense* microburst.

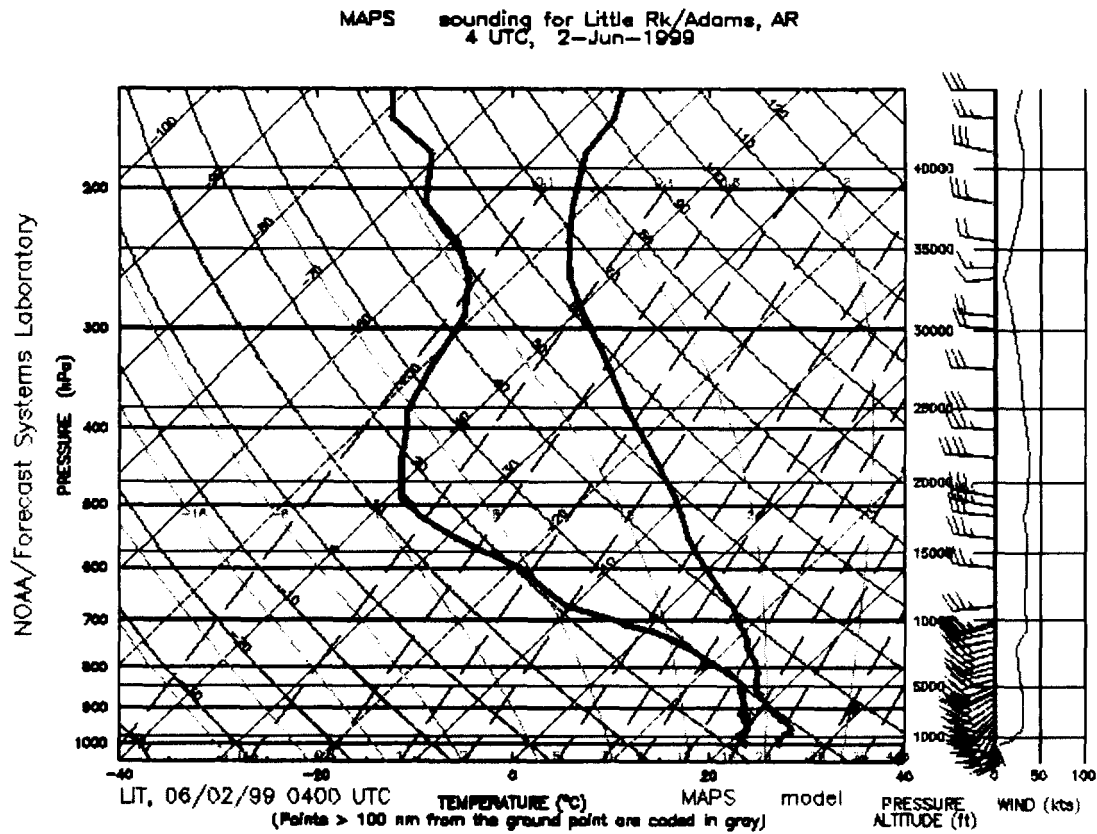


Figure 3. Thermodynamic diagram of sounding for Little Rock at 4:00 UTC on 2 June 1999. Generated from the MAPS weather forecast model (sounding and data provided by NOAA FSL).

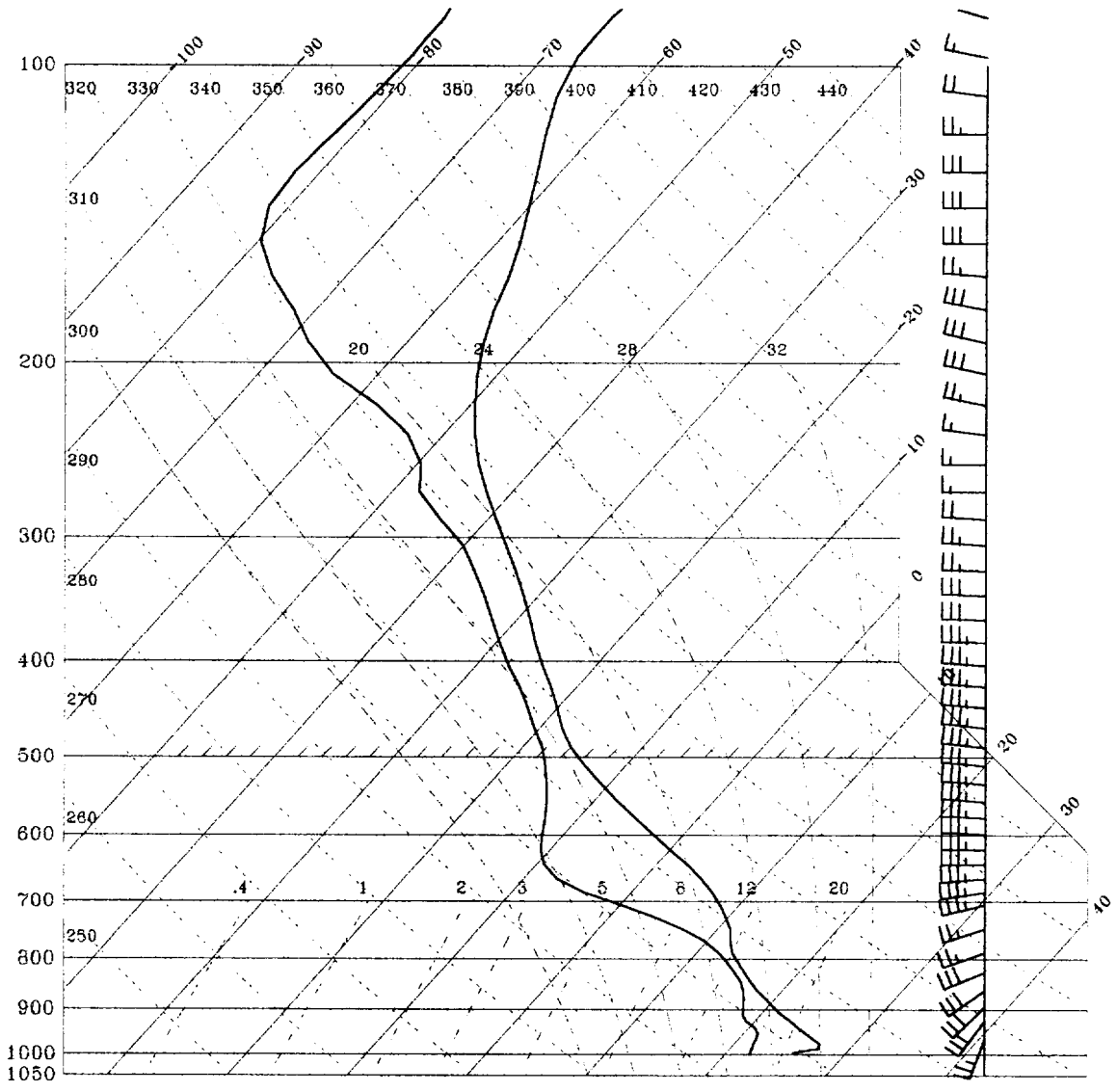


Figure 4. Modified MAPS sounding for Little Rock accident case. Assumed as input for Little Rock bow echo simulation.

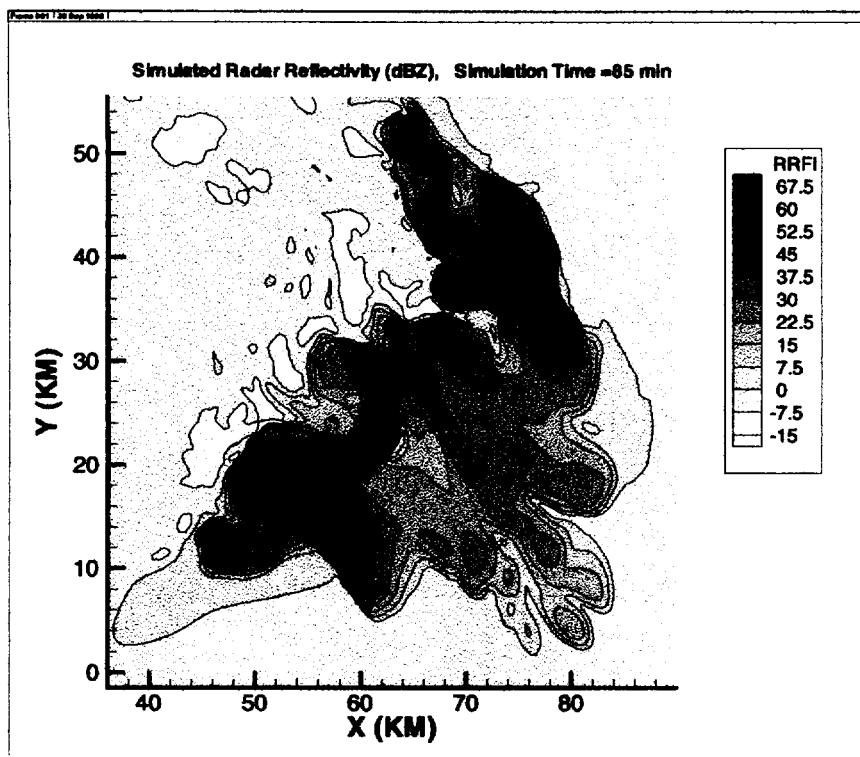


Figure 5. Horizontal cross section of radar reflectivity from TASS simulation. Field is at 900 m elevation and at 85 min.

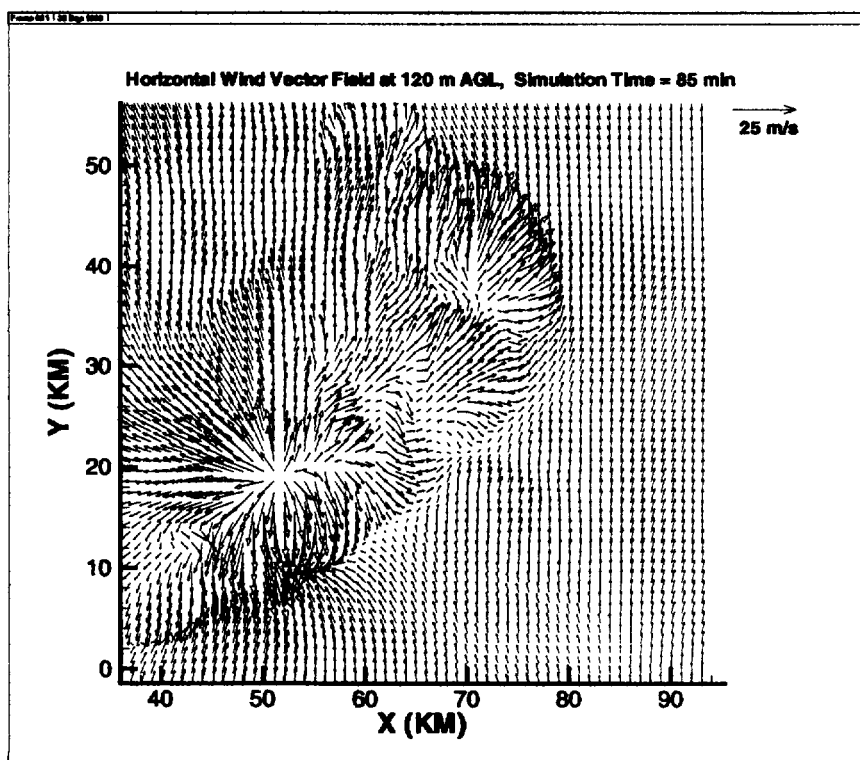


Figure 6. Simulated horizontal wind vector field at 120 m elevation and at 85 min.

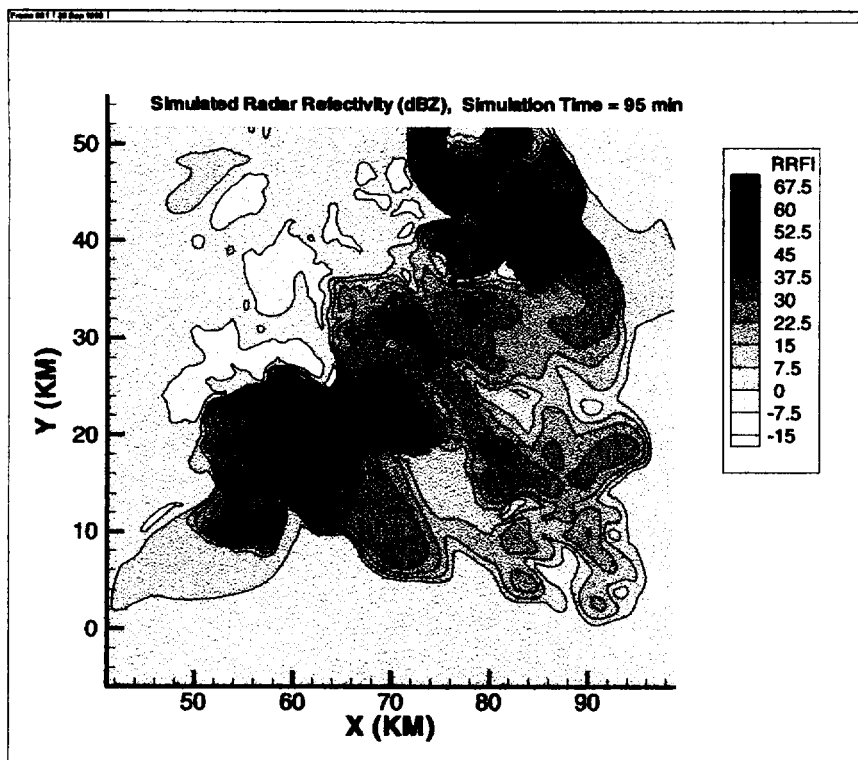


Figure 7. Same as Fig. 5, but for 95 min.

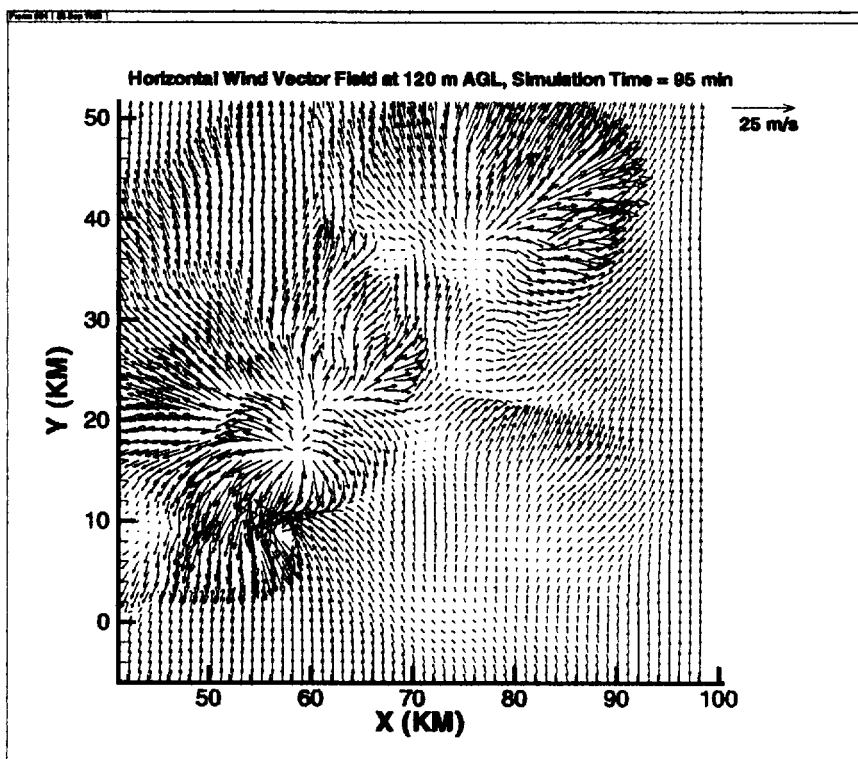


Figure 8. Same as Fig. 6, but for 95 min.

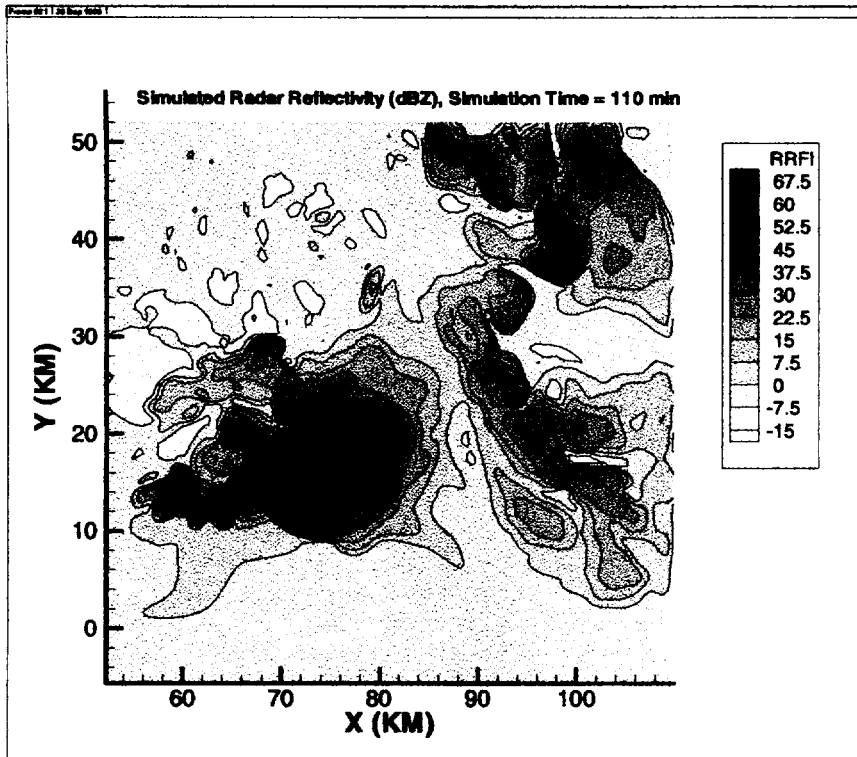


Figure 9. Same as Fig. 5, but for 110 min.

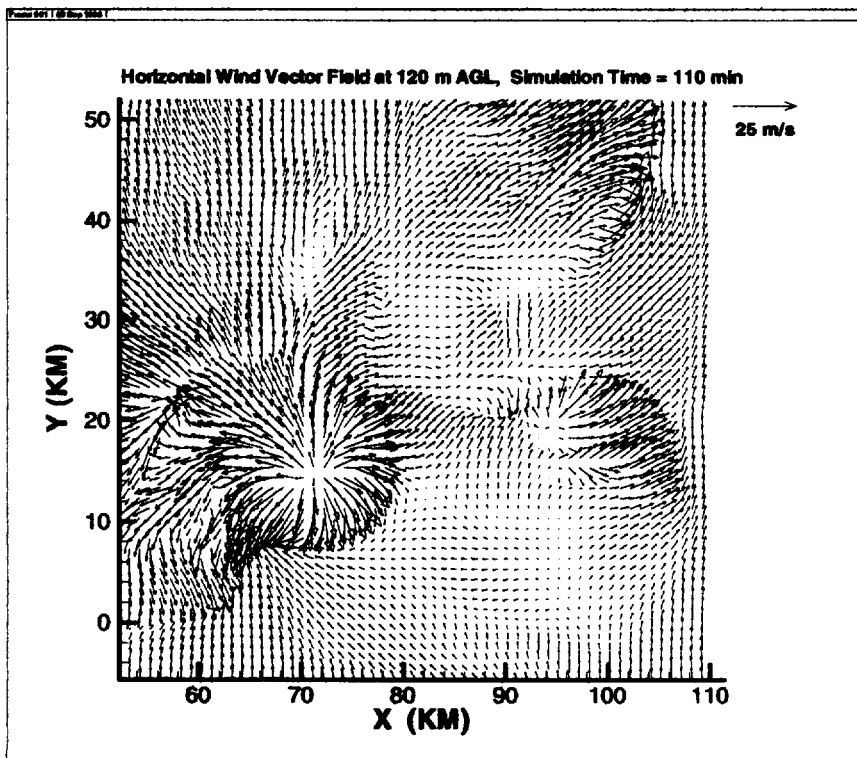


Figure 10. Same as Fig. 6, but for 110 min.